

## Article

# High-Strength Optical Coatings for Single-Crystal ZnGeP<sub>2</sub> by the IBS Method Using Selenide and Oxide Materials

Mikhail Zinovev <sup>1,\*</sup>, Nikolay N. Yudin <sup>1</sup>, Vladimir Kuznetsov <sup>2</sup>, Sergey Podzyvalov <sup>1</sup>, Andrey Kalsin <sup>1</sup>, Elena Slyunko <sup>1</sup>, Alexey Lysenko <sup>1</sup>, Denis Vlasov <sup>1</sup> and Houssain Baalbaki <sup>1</sup>

<sup>1</sup> Radiophysical Department, Laboratory of Radiophysical and Optical Methods for Studying the Environment, National Research Tomsk State University, 634050 Tomsk, Russia

<sup>2</sup> Institute of High Current Electronics, Akademichesky av. 2/3, 634055 Tomsk, Russia

\* Correspondence: muxa9229@gmail.com; Tel.: +7-952-158-37-58

**Abstract:** The paper presents the results on the development of an optical coating for a single-crystal ZnGeP<sub>2</sub> substrate based on a selenide-oxide pair of materials (ZnSe/Al<sub>2</sub>O<sub>3</sub>). The obtained coating ensures the operation of OPO in the mid-IR range up to 5 μm wavelengths. The possibility of ZnSe sputtering by the IBS method is shown. The obtained optical coating has a high laser-induced damage threshold (LIDT) value at a 2097 μm wavelength:  $W_0^E = 3.51 \text{ J/cm}^2$  in energy density and  $W_0^P = 101 \text{ W/cm}^2$  in power density at a 10 KHz pulse repetition frequency and a pulse duration of 35 ns. Thus, it is shown for the first time that the pair of materials ZnSe/Al<sub>2</sub>O<sub>3</sub> can be used for the deposition of optical coatings by the IBS method with high LIDT values for ZnGeP<sub>2</sub> optical elements operating in the mid-IR range.

**Keywords:** AR coatings; ZnSe; ion beam sputtering; oxides; ZnGeP<sub>2</sub> single crystal; LIDT



**Citation:** Zinovev, M.; Yudin, N.N.; Kuznetsov, V.; Podzyvalov, S.; Kalsin, A.; Slyunko, E.; Lysenko, A.; Vlasov, D.; Baalbaki, H. High-Strength Optical Coatings for Single-Crystal ZnGeP<sub>2</sub> by the IBS Method Using Selenide and Oxide Materials. *Ceramics* **2023**, *6*, 514–524. <https://doi.org/10.3390/ceramics6010030>

Academic Editor: Gilbert Fantozzi

Received: 17 November 2022

Revised: 10 January 2023

Accepted: 10 February 2023

Published: 13 February 2023



**Copyright:** © 2023 by the authors. Licensee MDPI, Basel, Switzerland. This article is an open access article distributed under the terms and conditions of the Creative Commons Attribution (CC BY) license (<https://creativecommons.org/licenses/by/4.0/>).

## 1. Introduction

The technologies of laser sources in the mid-IR range have made noticeable progress over the past few decades. The most efficient mid-IR sources are solid-state lasers [1], optical parametric oscillators (OPOs) [2–5], laser diodes [6,7], and quantum cascade lasers [8]. High-power OPOs in the mid-IR range are currently represented by nonlinear optical crystals KTP, KTA, ZnGeP<sub>2</sub>, GaSe, etc. [9–11]. Since there are large Fresnel reflection losses for ZnGeP<sub>2</sub> R~25% (one side), antireflection coatings are necessary for its practical application [12]. To significantly increase the efficiency of OPO, stringent requirements are imposed on the residual reflection and LIDT of such coatings.

The deposition of anti-reflection coatings is a complex and multi-stage process that includes many parameters. The method of deposition of optical films onto the substrate and the materials of coating are considered the fundamental parameters, especially in the manufacturing of laser optics operating in the IR range, where it is necessary to obtain high LIDT values.

Ion beam sputtering (IBS) [13] is a deposition method of interference coating with a high LIDT value and dense films with a high-refractive index, which are also characterized by high LIDT values [14–17]. The IBS method mainly sputters a pure metal target (Ta, Nb, Al, etc.) by supplying the sputtering chamber with a reactive gas (oxygen) and their oxide targets (for example, Ta<sub>2</sub>O<sub>5</sub>, Nb<sub>2</sub>O<sub>5</sub>, Al<sub>2</sub>O<sub>3</sub>, etc.) [14,15]. The approaches described in [17,18] also make it possible to sputter sulfide and fluoride ceramic targets using the IBS method. In previous work [18], the possibility of applying an optical anti-reflection coating with a high LIDT value on a ZnGeP<sub>2</sub> (hereinafter ZGP) substrate was presented. However, it has been shown that the specific sputtering rate of ZnS and YbF<sub>3</sub> by the IBS method is low [18]; as a result, the sputtering process requires a long time, which causes a negative effect where pollutants and residual gas, in the volume of the sputter chamber, get into the anti-reflective coating, which can significantly affect LIDT. At the same time, in

the operating range of the laser system, up to 5  $\mu\text{m}$ , it is possible to use the low-refractive oxide material  $\text{Al}_2\text{O}_3$  with ZnS, as shown in [19]. However, the problem of low sputtering rate of high-refractive ZnS still persists.

Based on physical and chemical parameters, the most suitable material with similar characteristics to ZnS is zinc selenide (ZnSe). This material is actively used to create resonator windows and filters for systems operating in the range of 2–14  $\mu\text{m}$  (material transparency region) [20]. Additionally, there are practically few studies on sputtering this material and creating AR coatings from it. Basically, this material is sputtered by thermal evaporation from molybdenum boats [21] and by the electron beam evaporation [22]. There is information in the literature about the LIDT of ZnSe thin films. For example, in [23], it is shown that its LIDT is in the range of 1–3  $\text{J}/\text{cm}^2$ , at a pulse repetition rate of 1 Hz. At the same time, in [24], an AR coating based on a ZnSe/YbF<sub>3</sub> pair shows LIDT at a level of 12.2  $\text{J}/\text{cm}^2$ . Additionally, ZnSe/YbF<sub>3</sub> structures on CaF<sub>2</sub> substrates by the e-beam evaporation method obtained Bloch surface waves [25] and deformable mirrors [26]. The production of ZnSe/ $\text{Al}_2\text{O}_3$  nanostructures and the study of their optical properties were conducted in [27] by RF magnetron sputtering on single-crystal silicon. However, the above studies did not use the IBS method for ZnSe sputtering and the creation of an AR coating on its basis in a pair with oxide. Therefore, the aim of this work is to study and refine the modes of ZnSe sputtering by the IBS method, as well as to develop an optical anti-reflection coating for a ZGP single-crystal substrate with a high LIDT value and a high sputtering rate based on a pair of ZnSe/ $\text{Al}_2\text{O}_3$  materials.

## 2. Substrate and Sputtering Equipment

As a substrate, a ZGP single crystal with dimensions of  $6 \times 6 \times 20 \text{ mm}^3$  (Figure 1) was used, which was cut from a ZGP single-crystal boule (manufactured by LOC LLC, Tomsk, Russia) at angles  $\theta = 54.5^\circ$  and  $\varphi = 0^\circ$  relative to optical axis. The ZGP single crystal boule was grown by the Bridgman method in the vertical direction on an oriented seed.

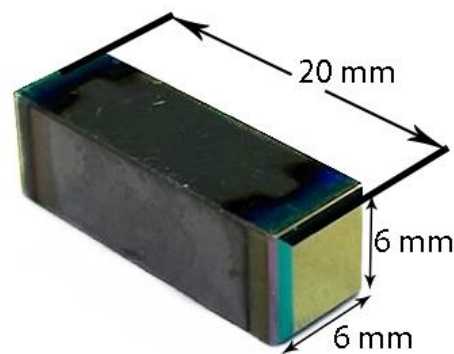


**Figure 1.** The photograph of ZGP OPO element with ZnSe/ $\text{Al}_2\text{O}_3$  AR coating.

Working surfaces were polished by the technology described [28]. The working surfaces of the samples were processed on a 4-PD-200 (Tomsk, Russia) polishing and finishing polish machine. Using this polishing machine, a laser quality polish was reached. The initial treatment of the working surfaces of all samples consisted of polishing on a cambric polishing pad using synthetic diamond powder DSF 0.5/0 (Diamond Synthetic Fine, average grain size 270 nm). In this case, the material removal was  $\sim 30 \mu\text{m}$ , which made it possible to remove the cracked layer formed in the process of cutting the crystal into oriented plates and their preliminary grinding—the polishing procedure. Next, the samples were polished on a cambric polishing pad using synthetic diamond powder DSF 0.25/0. Next, the samples were polished on a resin polishing pad made from polishing resin using DSF 0.25/0 synthetic diamond powder. The obtained samples were washed with cotton swabs and high purity acetone. Before applying interference coatings, the control of the profile of the working surfaces of the studied samples was carried out using a ZYGO NewView 7300 profilometer operating on the basis of white light interferometry. The

polishing of all the elements under study was carried out in a block; therefore, to evaluate such parameters as the maximum difference in height and depth of inhomogeneities on the surface (Pz), RMS depth of roughness (Pa) was selected from one of the samples. Its surface areas of  $110 \times 90 \mu\text{m}$  in size were studied, which showed the following results:  $Pz = 31.372 \text{ nm}$ ,  $Pa = 0.442 \text{ nm}$  (Figure 2).

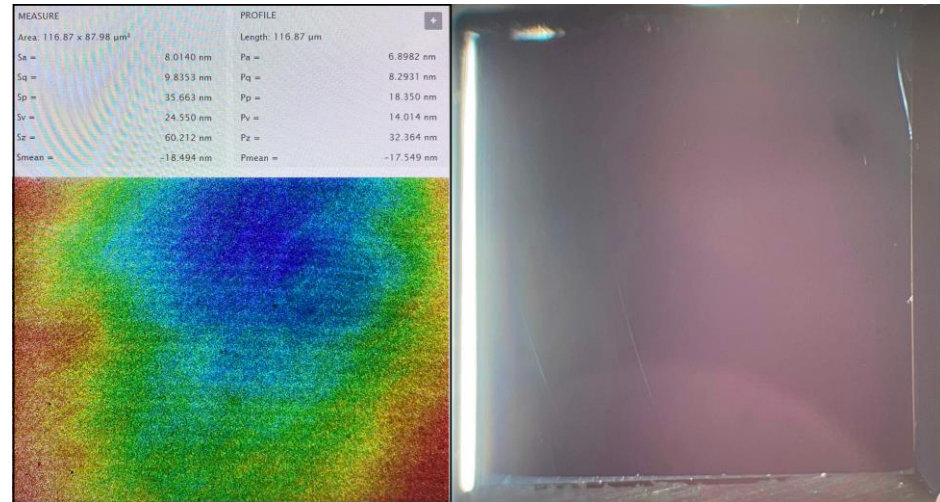


**Figure 2.** Parameters of polish quality. **Left**—image from profilometer, **right**—image from optical microscope.

Before loading into the sputter chamber, the substrates were cleaned using high purity acetone and then washed with bidistilled water. An anti-reflection coating was applied to the polished surfaces of the sample using the IBS method.

In this work, a vacuum-sputtering machine Aspira-200 manufactured by IZOVAC, Belarus, was used. The sputtering machine is equipped with an annular ion source (accelerator with anode layer), which has the ion-energy of 400–1500 eV (Figure 3, left). The maximum voltage of the ion source reaches 4.5 kV. An auxiliary ion source with an ion-energy of 100–1000 eV and a maximum voltage of 3 kV was used for ion purification ( $\sim 150 \text{ eV}$  energy was chosen). By this source, the substrate surface was cleaned from contaminants directly inside the chamber before the deposition of the anti-reflection coating.

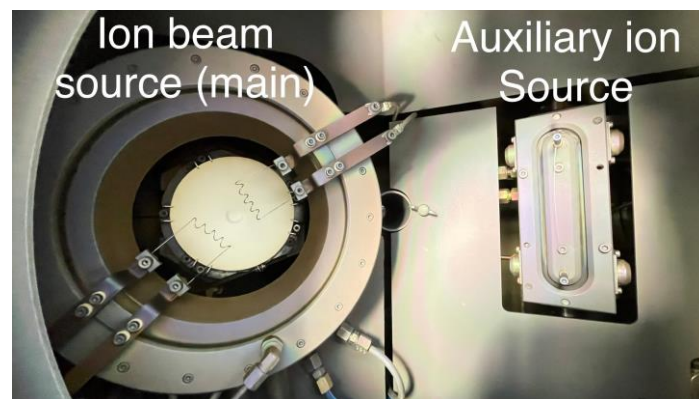


**Figure 3.** The image of an annular ion source (**left**) and auxiliary ion source (**right**).

A series of experiments was also carried out to determine the modes of compensation of the ionic charge on the surface of the target and substrates. It was found that when the ratio of the discharge current to the emission current from the hot cathodes is 1/1.3 (the emission current of the hot cathodes is 30% higher than the discharge current), the ion charge is completely compensated. When deviating from the obtained ratio, we

observed the following: when the ionic charge was undercompensated, defective structures of breakdowns by uncompensated heavy argon ions appeared in the film, and when overcompensated, an electronic breakdown of growing films occurred with the appearance of a “starry sky”-type defect, recorded with a profilometer (Figure 4, left) and an optical microscope (Figure 4, right).

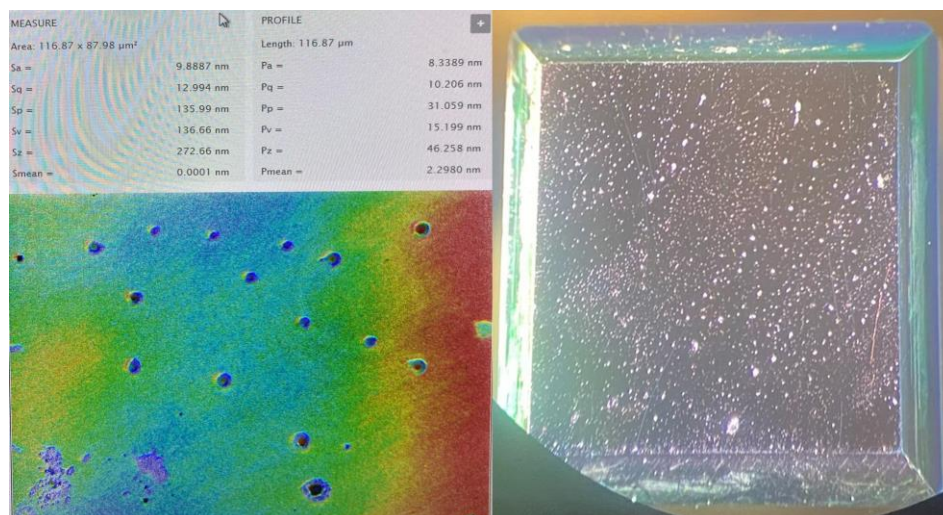


**Figure 4.** An electronic breakdown of crystal surface. **Left**—image from profilometer, **right**—image from optical microscope.

The deposition equipment provides heating for the substrate up to 300 °C. However, during the deposition process, the substrate temperature was maintained at 100 °C. It was impossible to use higher temperatures due to the limitation imposed by the substrate because at temperatures above 100 °C, annealing of the material and damage to optical characteristics may occur. High-purity argon (AR 99.995%) was chosen as the working gas. The sputtering targets were disks with a diameter of  $\varnothing 101.6$  mm and a thickness of 6 mm. A ZnSe single-crystal target with a purity of 99.999% (5N), manufactured by Electrosteklo LLC, Russia, was chosen as a high-refractive material. An Alumina metal target with a purity of 99.999% (5N), produced by Xing Kang coating materials, China, was chosen as a low-refractive material.

### 3. AR Coating Design

To develop AR coating, firstly, single layers of materials, from which we later developed an interference coating, were studied. ZnSe was used as a high-refractive layer, and  $\text{Al}_2\text{O}_3$  was used as a low-refractive layer. The deposition parameters of the studied materials are presented in Table 1.

**Table 1.** Deposition parameters of the chosen materials.

Sputtering Target	Accelerating Voltage of the Ion Source, kV (Ion Energy in Ev)	Layer Deposition Rate, nm/s	Residual Pressure in the Chamber at the Beginning of the Sputtering Process, Pa	Working Pressure in the Chamber during Sputtering, Pa	Used Gas/Flow, $\text{cm}^3$ per mSin
$\text{Al}_2\text{O}_3$	3.5 (1200)	0.1	$5 \times 10^{-4}$	$5 \times 10^{-2}$	Ar/18 O <sub>2</sub> /20
ZnSe	2.5 (900)	0.09	$5 \times 10^{-4}$	$3.3 \times 10^{-2}$	Ar/15

The selection of spraying modes was carried out using electronic gas flow meters, as well as accelerating voltage at the source. The optimal ratios of the Ar/O<sub>2</sub> gas mixture for the  $\text{Al}_2\text{O}_3$  monolayer were selected, at which a low optical absorption was observed in the studied samples, and a high sputtering rate and film density were achieved (determined from the change in the refractive index). Only argon gas was used to sputter the ZnSe target.

Thus, we obtained the following gas regimes for the materials under study, presented in Table 1.

With such configurations of gas supply and voltages, an optimal ratio of the deposition rate to the quasi-stoichiometry of the film composition (determined indirectly, by the refractive index), its adhesion to the substrate, and mechanical strength were observed. In the case of oxide materials, a change in the Ar value in the gas mixture led to an increase in the optical absorption in the films. An increase in O<sub>2</sub> in the mixture led to a significant (up to 2 times) decrease in the sputtering rate due to the “acidification” of the target and the formation of an oxide film on its surface.

As can be seen from Table 1, the rate of deposition of the Al<sub>2</sub>O<sub>3</sub> layer is about 0.1 nm/s, which is approximately 5 times higher than the rate of deposition of the YbF<sub>3</sub> layer (equal to 0.02 nm/s [18]) when targets were sputtered by the IBS method. The sputtering rate of the high-refractive ZnSe material was ~0.09 nm/s, twice as high as ZnS, the sputtering rate of which is 0.04–0.045 nm/s [18]. Thus, the time of sputtering process can be significantly reduced using Al<sub>2</sub>O<sub>3</sub> instead of YbF<sub>3</sub>, where possible, and ZnSe instead of ZnS.

Next, the dispersion characteristics of used materials was obtained. The refractive index dispersions, as well as the absorption of the layers, were calculated in the Optichar software module version 14.57 of the Optilayer software. The calculation was carried out according to the transmission and reflection characteristics of the layers under study deposited on BK8 optical glass (in the wavelength range of 400–2000 nm) and a germanium plate to describe them in the IR region. The thickness of the deposited single layers was about 1 μm. The transmission and reflection spectra were obtained using a Shimadzu UV-3600 Plus spectrometer (Shimadzu, Japan, Tokyo) and a Simex FT-801 Fourier spectrometer (Novosibirsk, Russia).

Figure 5 shows the refractive index dispersion and absorption of an Al<sub>2</sub>O<sub>3</sub> single layer.

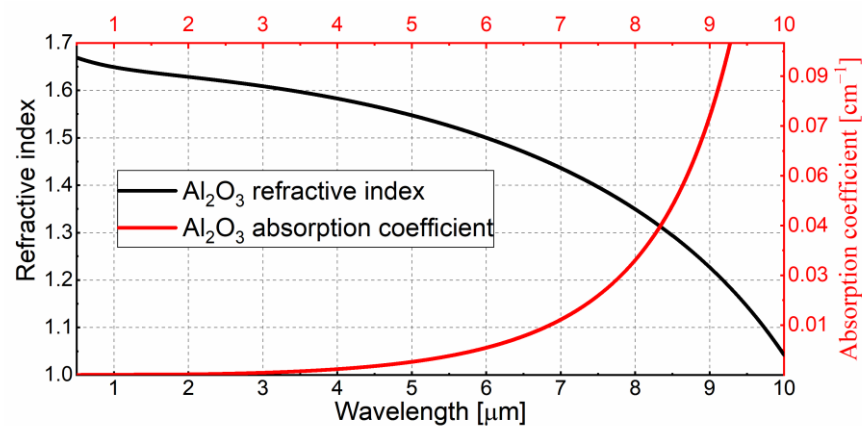
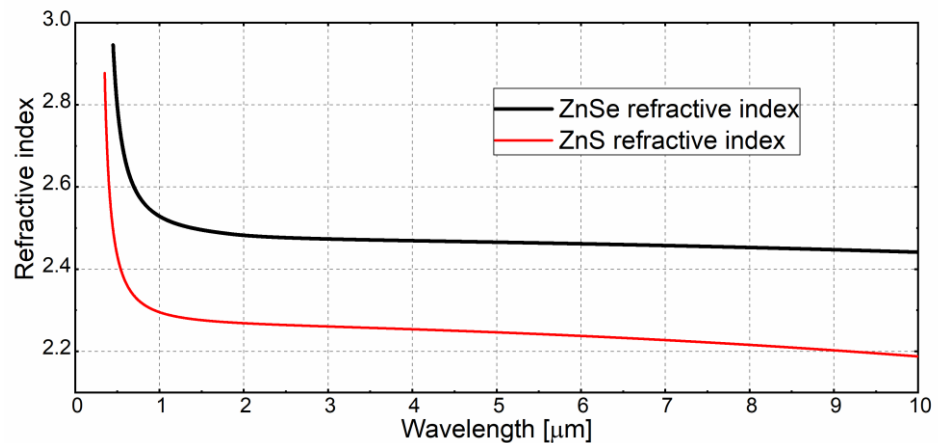


Figure 5. Refractive index and absorption of Al<sub>2</sub>O<sub>3</sub> single layer.

The refractive index dispersion of Al<sub>2</sub>O<sub>3</sub> changes slightly by  $\Delta n \sim 0.15$  in the visible wavelength range up to 6 μm. At the same time, in the range of wavelengths longer than 6 μm, a rather sharp decrease in the refractive index and a sharp increase in absorption are observed. This is due to the presence of a wide resonant absorption line in the range of 10–12 μm, due to the presence of M–O bonds [29]. Therefore, aluminum oxide can be used in the production of optical coatings operating in the IR range up to ~6 μm, and in relatively thin layers, less than  $\leq 1$  μm thick.

Then, the optical properties of the ZnSe single layer were determined. The refractive index dispersion is shown in Figure 6.



**Figure 6.** Refractive index of ZnSe (black) single layer and ZnS (red) single layer taken from [19].

According to the obtained dispersion, the refractive index of ZnSe changes slightly by  $\Delta n \leq 0.1$  in the range from 1.5  $\mu\text{m}$  to 12  $\mu\text{m}$  wavelengths. The sharp increase in the refractive index is associated with the presence of resonant absorption bands in the range of 250–270 nm [20]. This material is practically transparent in the range from 800 nm to 15–16  $\mu\text{m}$ . The absorption of a single layer is not shown in Figure 4 because it is not informative, as it is close to zero ( $\alpha \leq 10^{-6} \text{ cm}^{-1}$ ) in the range of 1–12  $\mu\text{m}$ . It should also be noted that the refractive index agrees well with the obtained data in [30]. As shown in Figure 4, the difference in refractive index dispersions for ZnSe and ZnS layers is  $\Delta n \geq 0.2$ .

Using the obtained optical characteristics of the materials, a three-layer AR coating was calculated for the ZGP substrate according to the scheme  $\text{sub} | 0.94 \text{ L } 2.69 \text{ H } 5.23 \text{ L} |$ , where L is the low-refractive layer, H is the high-refractive layer, and sub is the ZGP substrate. A control wave of 600 nm was chosen. An incident angle of  $0^\circ$  was chosen and an average polarization Ra was used. The operating band of the coating was chosen to generate OPO on ZGP in the range of 3500–5000 nm, pumped with 2097 nm of radiation. The calculated coating was deposited on a ZGP single crystal (Figure 1), and on a ZGP control plate, one of its sides was matte. The characteristics of the calculated and measured coating, as well as its spectra, are presented in Table 2 in Figure 7.

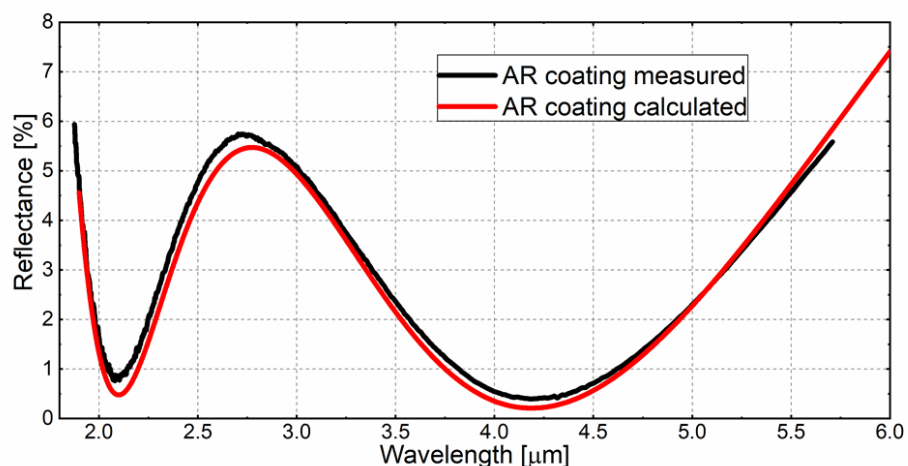


**Figure 7.** Reflection spectra of AR coating (ZnSe/ $\text{Al}_2\text{O}_3$ ): red—calculated in Optilayer; black—measured.

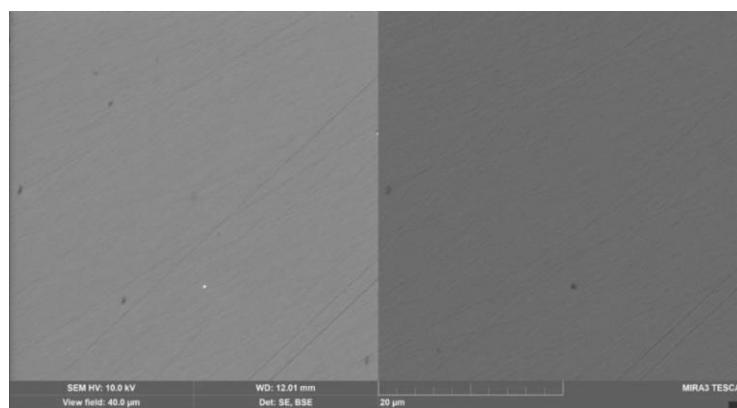
**Table 2.** Characteristics of the calculated coating.

Materials Used	Target Operating Range, in nm (Wavelength)	Number of Layers in the Designed Coating	Total Coating Thickness, nm
ZnSe/Al <sub>2</sub> O <sub>3</sub>	$R \leq 1\%$ , on 2097/ $R \leq 2\%$ , on 3500–5000	3	721

As can be seen from Figure 7, the measured reflection spectrum of the AR coating has some differences from the calculated one. This is due to the presence of residual reflection from the matted surface of the substrate and the error in determining the refractive index dispersion, in addition to the error in the layer thickness during deposition, which occurs due to the lack of a quartz sensor for measuring the thickness of the sputtered layer inside the chamber, The control of the sputtered coating was carried out by optical transmission methods.

The obtained coating satisfies the target characteristics indicated in Table 2. Using ZnSe instead of ZnS allowed us to reduce the thickness of the high-refractive layer by 65%, from 264 nm to 154 nm, while maintaining the optical characteristics of the coating, with a slight change in the thicknesses of the low-refractive layer. This reduced the deposition time from 5 to 3 h, that is, by ~30%. The LIDT of the obtained coating on the ZGP substrate was tested using a Ho:YAG laser The measurement results are shown below.

During the work, the morphology of the deposited interference coating was determined on a Tescan MIRA 3 LMU scanning electron microscope with a Schottky cathode. Scanning was performed at an accelerating voltage (HV) of 10 kV. The samples were coated with a carbon conductive coating using a Quorum Technologies EMITECH K450X setup (Quorum Technologies, Laughton, UK). As studies have shown, in the sample, in the layers of defects in the interference antireflection coating, no defective structure of the film was found; only defects in the surface layer of the substrate, scratches and dents after polishing, shown in Figure 8, were found.

**Figure 8.** The morphology of the deposited interference coating determined by Tescan MIRA 3 LMU.

#### 4. LIDT Test of AR-Coated OPO

The block-scheme of the laser system used in the experiment in the LIDT test in Figure 9 is shown. The Ho:YAG laser with a wavelength of 2097 nm, pulse repetition rate of 10 kHz, pulse duration of 35 ns, and with p-polarization was used. The measured diameter of the laser beam on the input crystal surface was  $d = 350 \mu\text{m}$  at the  $e^{-2}$  level of the maximum intensity in all experiments. The maximum average radiation power generated by the Ho:YAG laser was 20 W in a linearly polarized Gaussian beam (parameter  $M^2 \leq 1.3$ ). The output laser power could be controlled by the system of the polarizer (1) and BSC (2) by the rotation of polarizer (1).

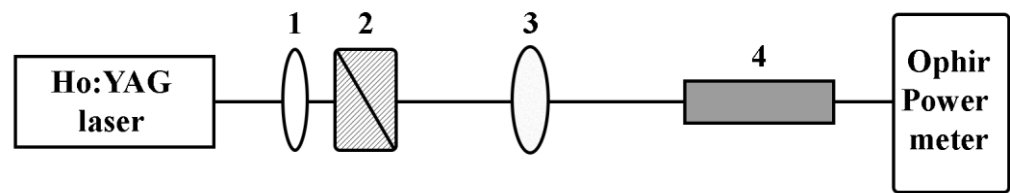


**Figure 9.** The block-scheme of laser system used in experiment (LIDT test): 1—polarizer; 2—beam-splitter cube (BSC); 3—focusing lens with focal distance 200 mm; 4—investigated ZGP element.

To determine the LIDT of the investigated samples, the “R-on-1” method was used according to the ISO standard described in detail in [10,11], which requires less space on the sample surface compared to the “S-on-1” method and, therefore, can be applied to samples with a limited aperture, but is considered more rough. The essence of this technique lies in the fact that each individual region of the crystal is irradiated with laser radiation with a successive increase in the intensity of laser radiation until an optical breakdown occurs or a predetermined energy density value is reached. In our work, the study was carried out with an exposure duration of laser radiation  $\tau_{\text{ex}} = 10$  s. The sample under study was exposed to packets of laser pulses with a fixed level of energy density that did not cause damage to the surface of the crystals. Further, the energy density level increased with a step of  $\sim 0.1$  J/cm<sup>2</sup>. When visible damage appeared on one of the surfaces of the nonlinear element, the experiment was terminated. Then, the sample was moved by 0.8 mm in height or width using a two-coordinate shift. The experiment was repeated 10 times. The optical breakdown probability was obtained by plotting the cumulative probability as a function of the optical breakdown energy density. The value of LIDT ( $W_0$ ) was taken to be the energy density corresponding to the leading approximation of the probability of optical breakdown to zero.

Three samples were tested: (1) without AR coating; (2) with AR coating ZnS/Al<sub>2</sub>O<sub>3</sub>; (3) with AR coating ZnSe/Al<sub>2</sub>O<sub>3</sub>. The measurement results are shown in Figure 10. The measurements were carried out on a sample of 10 points for each sample, and the statistical error in determining the LIDT value is also given. Damage (crystal breakdown) was recorded by a sharp drop in the radiation power on the power meter, as well as by the glow of ionized ejection products from the surface and a characteristic sound. Then, the damage to the surface was fixed in an optical microscope. In the graphs presented, the ordinate shows the probability of optical breakdown in relative units, normalized to unity, and the abscissa shows the energy density of the testing laser radiation.

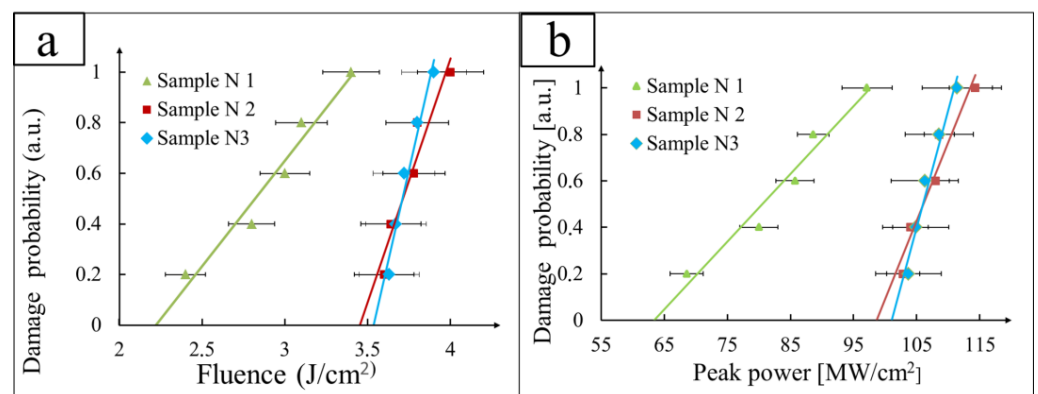


**Figure 10.** (a) is the dependence of the optical breakdown probability on the energy density of the testing laser radiation; (b) is the dependence of the optical breakdown probability on the power density of the testing laser radiation. The results were obtained at a pulse repetition rate of 10 kHz and a pulse duration of 35 ns.

Thus, the LIDT of sample No. 1 (without antireflection coatings) was  $W_0^E = 2.23 \text{ J/cm}^2$  and  $W_0^P = 64 \text{ W/cm}^2$ , where  $W_0^E$  is LIDT in energy density and  $W_0^P$  is expressed in power density. The LIDT of sample No. 2 (ZnS/Al<sub>2</sub>O<sub>3</sub>) was  $W_0^E = 3.45 \text{ J/cm}^2$  and  $W_0^P = 99 \text{ W/cm}^2$ . The optical breakdown threshold of sample No. 3 (ZnSe/Al<sub>2</sub>O<sub>3</sub>) was  $W_0^E = 3.51 \text{ J/cm}^2$  and  $W_0^P = 101 \text{ W/cm}^2$ . As in our previous work [11], an increase by 1.5 times in LIDT was observed after the deposition of antireflection coatings based on ZnSe and Al<sub>2</sub>O<sub>3</sub> materials. The selected pairs of materials have physicochemical properties that promote good adhesion of the multilayer coating to the polished crystal surface and minimal mechanical stresses between the layers and at the substrate/film interface, which, as a result, leads to an increase in LIDT. An adhesion test was carried out using ISO 9211-4:2012 “Optics and photonics-Optical coatings-Part 4: Specific test methods”.

## 5. Conclusions

In this work, an antireflection coating was developed for the ZGP single crystal substrate based on a high-refractive ZnSe layer and a low-refractive Al<sub>2</sub>O<sub>3</sub>.

It has been shown that a zinc selenide (ZnSe) material can be successfully sputtered by the IBS method, and the refractive index of the resulting ZnSe film was determined in a wide range of wavelengths. It was found that the sputtering rate of the ZnSe material is 2 times higher than the sputtering rate of the ZnS material when using the IBS method, which allowed it to reduce the deposition time of the AR coating by ~30%. The LIDT ZGP with AR coatings on the working surfaces was determined by the “R-on-1” method, which was  $W_0^E = 3.51 \text{ J/cm}^2$  expressed by energy density and  $W_0^P = 101 \text{ W/cm}^2$  expressed by power density. An increase in the LIDT value by 1.5 times between non-coated and AR-coated samples is observed. The observed differences in the LIDT values may be due to the redistribution of the electromagnetic field on the surface of the sample due to the deposition of an antireflection coating on it. Additionally, chosen pairs of materials (ZnSe/Al<sub>2</sub>O<sub>3</sub>) have physicochemical properties that promote good adhesion of the multilayer coating to the polished crystal surface and minimal mechanical stresses between the layers and at the substrate/film interface due to ZnSe, a relatively soft material with a Mohs hardness of ~3–4. This value is slightly lower than that of the ZGP crystal, which has a hardness of ~5.

**Author Contributions:** Conceptualization, M.Z., N.N.Y. and V.K.; methodology, A.K. and E.S.; software, M.Z. and V.K.; validation, E.S. and S.P.; formal analysis, N.N.Y. and A.L.; investigation, M.Z., V.K. and N.N.Y.; resources, D.V.; data curation, A.K. and V.K.; writing—original draft preparation, M.Z.; writing—review and editing, N.N.Y., V.K. and H.B.; supervision, M.Z.; project administration M.Z.; funding acquisition, M.Z. and N.N.Y. All authors have read and agreed to the published version of the manuscript.

**Funding:** This study was supported by the Tomsk State University Development Program (Priority 2030).

**Institutional Review Board Statement:** Not applicable.

**Informed Consent Statement:** Not applicable.

**Data Availability Statement:** Not applicable.

**Conflicts of Interest:** The authors declare no conflict of interest. The funders had no role in the design of the study; in the collection, analyses, or interpretation of data; in the writing of the manuscript; or in the decision to publish the results.

## References

1. Sorokina, I.; Vodopyanov, K. *Solid-State Mid-Infrared Laser Sources*; Springer: Berlin/Heidelberg, Germany, 2003; p. 557; ISSN 1437-0859. [[CrossRef](#)]
2. Wang, L.; Xing, T.; Hu, S.; Wu, X.; Wu, H.; Wang, J.; Jiang, H. Mid-infrared ZGP-OPO with a high optical-to-optical conversion efficiency of 75.7%. *Opt. Express* **2017**, *25*, 3373–3380. [[CrossRef](#)]
3. Wu, R.; Lai, K.; Wong, H.; Xie, W.; Lim, Y.; Lau, E. Multiwatt mid-IR output from a Nd: YALO laser pumped intracavity KTA OPO. *Opt. Express* **2001**, *8*, 694–698. [[CrossRef](#)]

4. Fu, Q.; Xu, L.; Liang, S.; Shardlow, P.C.; Shepherd, D.P.; Alam, S.U.; Richardson, D.J. High-average-power picosecond mid-infrared OP-GaAs OPO. *Opt. Express* **2020**, *28*, 5741–5748. [[CrossRef](#)]
5. Henriksson, M.; Tiihonen, M.; Pasiskevicius, V.; Laurell, F. Mid-infrared ZGP OPO pumped by near-degenerate narrowband type-I PPKTP parametric oscillator. *Appl. Phys. B* **2007**, *88*, 37–41. [[CrossRef](#)]
6. Sun, G.; Soref, R.; Cheng, H. Design of a Si-based lattice-matched room-temperature GeSn/GeSiSn multi-quantum-well mid-infrared laser diode. *Opt. Express* **2010**, *18*, 19957–19965. [[CrossRef](#)]
7. Tournié, E.; Baranov, A.N. Chapter 5—Mid-Infrared Semiconductor Lasers: A Review. In *Semiconductors and Semimetals*; Elsevier: Amsterdam, The Netherlands, 2012; Volume 86, pp. 183–226; ISSN 0080-8784. ISBN 9780123910660. [[CrossRef](#)]
8. Yao, Y.; Hoffman, A.; Gmachl, C. Mid-infrared quantum cascade lasers. *Nat. Photonics* **2012**, *6*, 432–439. [[CrossRef](#)]
9. Žendzian, W.; Jabczyński, J.; Wachulak, P.; Kwiatkowski, J. High-repetition-rate, intracavity-pumped KTP OPO at 1572 nm. *Appl. Phys. B* **2005**, *80*, 329–332. [[CrossRef](#)]
10. Haakestad, M.W.; Fonnum, H.; Lippert, E. Mid-infrared source with 0.2 J pulse energy based on nonlinear conversion of Q-switched pulses in ZnGeP<sub>2</sub>. *Opt. Express* **2014**, *22*, 8556–8564. [[CrossRef](#)]
11. Murphy, F.J.; Amrania, H.; Phillips, C.C. Widely Tunable Midinfrared Radiation from GaSe OPO. *Nonlinear Opt. B* **2013**, NW4A.21. [[CrossRef](#)]
12. Aydin, C.; Zaslavsky, A.; Sonek, G.; Goldstein, J. Reduction of reflection losses in ZnGeP<sub>2</sub> using motheye antireflection surface relief structures. *Appl. Phys. Lett.* **2002**, *80*, 2242–2244. [[CrossRef](#)]
13. Böntgen, T.; Alig, T.; Balasa, I.; Jensen, L.; Ristau, D. Advances in IBS Coatings for space applications on the topics of curved surfaces and laser damage. In Proceedings of the International Conference on Space Optics, Chania, Greece, 9–12 October 2018; SPIE: Bellingham, WA, USA, 2019; Volume 11180, pp. 1539–1545.
14. Liu, H.; Jensen, L.; Ma, P.; Ristau, D. Stress compensated anti-reflection coating for high power laser deposited with IBS SiO<sub>2</sub> and ALD Al<sub>2</sub>O<sub>3</sub>. *Appl. Surf. Sci.* **2019**, *476*, 521–527. [[CrossRef](#)]
15. Cheng, X.J.; Zhao, Y.; Qiang, Y.; Zhu, Y.; Guo, L.; Shao, J. Comparison of laser-induced damage in Ta<sub>2</sub>O<sub>5</sub> and Nb<sub>2</sub>O<sub>5</sub> single-layer films and high. *Chin. Opt. Lett.* **2011**, *9*, 013102.
16. Ribeaud, A.; Pistner, J.; Hagedorn, H.; Brophy, M.; Kupinski, P.; Watson, J.; Hand, R. Production of high laser induced damage threshold mirror coatings using plasma ion assisted evaporation, plasma assisted reactive magnetron sputtering and ion beam sputtering. In Proceedings of the Laser-Induced Damage in Optical Materials 2018: 50th Anniversary Conference, Boulder, CO, USA, 23–26 September 2018; SPIE: Bellingham, WA, USA, 2018; Volume 10805, pp. 134–142.
17. Ribeaud, A.; Pistner, J.; Hagedorn, H.; Joseph, S. Infra-Red Multi-Layer Coatings Using YbF<sub>3</sub> and ZnS in an Ion Beam Sputtering System. In Proceedings of the Optical Interference Coatings Conference (OIC), Santa Ana Pueblo, NM, USA, 2–7 June 2019; pp. 1–4.
18. Zinovev, M.; Yudin, N.N.; Kinyaevskiy, I.; Podzvalov, S.; Kuznetsov, V.; Slyunko, E.; Baalbaki, H.; Vlasov, D. Multispectral Anti-Reflection Coatings Based on YbF<sub>3</sub>/ZnS Materials on ZnGeP<sub>2</sub> Substrate by the IBS Method for Mid-IR Laser Applications. *Crystals* **2022**, *12*, 1408. [[CrossRef](#)]
19. Zinoviev, M.; Yudin, N.N.; Podzvalov, S.; Slyunko, E.; Yudin, N.A.; Kulesh, M.; Dorofeev, I.; Baalbaki, H. Optical AR Coatings of the Mid-IR Band for ZnGeP<sub>2</sub> Single Crystals Based on ZnS and Oxide Aluminum. *Crystals* **2022**, *12*, 1169. [[CrossRef](#)]
20. Adachi, S.; Taguchi, T. Optical properties of ZnSe. *Phys. Rev. B* **1991**, *43*, 9569. [[CrossRef](#)]
21. Venkatachalam, S.; Mangalaraj, D.; Narayandass, S.K. Characterization of vacuum-evaporated ZnSe thin films. *Phys. B Condens. Matter* **2007**, *393*, 47–55. [[CrossRef](#)]
22. Varasi, M.; Misiano, C.; Mancini, C.; Sartori, P. Plasma assisted ion plating deposition of optical thin films for coatings and integrated optical applications. *Vacuum* **1986**, *36*, 143–147. [[CrossRef](#)]
23. Zou, F.; Xun, J.; Su, J.; Ma, J. Influence of Laser-Conditioning on Laser-Induced Damage Properties of ZnSe Thin Films. *Adv. Mater. Res.* **2012**, *602–604*, 1437–1443. [[CrossRef](#)]
24. Rahe, M.; Ristau, D.; Schmidt, H. Effect of hydrogen concentration in conventional and IAD coatings on the absorption and laser-induced damage at 10.6 μm. In Proceedings of the 24th Annual Boulder Damage Symposium Proceedings—Laser-Induced Damage in Optical Materials, Boulder, CO, USA, 28–30 October 1992; SPIE: Bellingham, WA, USA, 1993; Volume 1848, pp. 335–348.
25. Smolik, G.; Descharmes, N.; Herzig, H. Observation of Bloch Surface Waves in the Mid-Infrared Spectral Range. In Proceedings of the 2018 International Conference on Optical MEMS and Nanophotonics (OMN), Lausanne, Switzerland, 29 July–2 August 2018; pp. 66–67.
26. Peng, J.; Hu, X.; Chen, L.; Zhang, B. Effect of Structural Parameters of Deformable Mirrors on Phase Characteristics of High-Power Laser. *Acta Opt. Sin.* **2015**, *35*, 0514001-1–0514001-9. [[CrossRef](#)]
27. Ivanov, M.M.; Zakirova, R.M.; Kobziev, V.F.; Krylov, P.N.; Fedotova, I.V. Properties of ZnSe/Al<sub>2</sub>O<sub>3</sub> Nanostructures Obtained by RF Magnetron Sputtering. *Tech. Phys.* **2018**, *63*, 1504–1506. [[CrossRef](#)]
28. Yudin, N.; Khudoley, A.; Zinoviev, M.; Podzvalov, S.; Slyunko, E.; Zhuravleva, E.; Kulesh, M.; Gorodkin, G.; Kumeysya, P.; Antipov, O. The Influence of Angstrom-Scale Roughness on the Laser-Induced Damage Threshold of Single-Crystal ZnGeP<sub>2</sub>. *Crystals* **2022**, *12*, 83. [[CrossRef](#)]

29. Wachs, I.E. Raman and IR studies of surface metal oxide species on oxide supports: Supported metal oxide catalysts. *Catal. Today* **1996**, *27*, 437–455. [[CrossRef](#)]
30. Amotchkina, T.; Trubetskov, M.; Hahner, D.; Pervak, V. Characterization of e-beam evaporated Ge, YbF<sub>3</sub>, ZnS, and LaF<sub>3</sub> thin films for laser-oriented coatings. *Appl. Opt.* **2020**, *59*, A40–A47. [[CrossRef](#)]

**Disclaimer/Publisher's Note:** The statements, opinions and data contained in all publications are solely those of the individual author(s) and contributor(s) and not of MDPI and/or the editor(s). MDPI and/or the editor(s) disclaim responsibility for any injury to people or property resulting from any ideas, methods, instructions or products referred to in the content.